OPEN ACCESS

University of BRISTOL

Sage, A. G., Oliver, T. A. A., King, G. A., Murdock, D., Harvey, J. N., & Ashfold, M. N. R. (2013). UV photolysis of 4-iodo-, 4-bromo-, and 4-chlorophenol: Competition between C-Y (Y = halogen) and O-H bond fission. *Journal of Chemical Physics*, *138*(16), [164318]. https://doi.org/10.1063/1.4802058

Publisher's PDF, also known as Version of record

Link to published version (if available):
10.1063/1.4802058

Link to publication record in Explore Bristol Research
PDF-document

Copyright (2013) American Institute of Physics. This article may be downloaded for personal use only. Any other use requires prior permission of the author and the American Institute of Physics. The following article appeared in A. G. Sage et al., J. Chem. Phys. 138, 164318 (2013) and may be found at; http://dx.doi.org/10.1063/1.4802058.

University of Bristol - Explore Bristol Research
General rights

This document is made available in accordance with publisher policies. Please cite only the published version using the reference above. Full terms of use are available:
http://www.bristol.ac.uk/red/research-policy/pure/user-guides/ebr-terms/

UV photolysis of 4-iodo-, 4-bromo-, and 4-chlorophenol: Competition between C–Y (Y = halogen) and O–H bond fission

Alan G. Sage, Thomas A. A. Oliver, Graeme A. King, Daniel Murdock, Jeremy N. Harvey et al.

Citation: J. Chem. Phys. **138**, 164318 (2013); doi: 10.1063/1.4802058
View online: http://dx.doi.org/10.1063/1.4802058
View Table of Contents: http://jcp.aip.org/resource/1/JCPSA6/v138/i16
Published by the American Institute of Physics.

Additional information on J. Chem. Phys.

Journal Homepage: http://jcp.aip.org/
Journal Information: http://jcp.aip.org/about/about_the_journal
Top downloads: http://jcp.aip.org/features/most_downloaded
Information for Authors: http://jcp.aip.org/authors

ADVERTISEMENT

Downloaded 30 Apr 2013 to 137.222.43.31. This article is copyrighted as indicated in the abstract. Reuse of AIP content is subject to the terms at: http://jcp.aip.org/about/rights_and_permissions

UV photolysis of 4-iodo-, 4-bromo-, and 4-chlorophenol: Competition between C–Y (Y = halogen) and O–H bond fission

Alan G. Sage, Thomas A. A. Oliver,[a] Graeme A. King,[b] Daniel Murdock, Jeremy N. Harvey, and Michael N. R. Ashfold[c]
School of Chemistry, University of Bristol, Bristol BS8 1TS, United Kingdom

(Received 15 February 2013; accepted 4 April 2013; published online 30 April 2013)

The wavelength dependences of C–Y and O–H bond fission following ultraviolet photoexcitation of 4-halophenols (4-YPhOH) have been investigated using a combination of velocity map imaging, H Rydberg atom photofragment translational spectroscopy, and high level spin-orbit resolved electronic structure calculations, revealing a systematic evolution in fragmentation behaviour across the series Y = I, Br, Cl (and F). All undergo O–H bond fission following excitation at wavelengths $\lambda \lesssim 240$ nm, on repulsive ($(n/\pi)\sigma^*$) potential energy surfaces (PESs), yielding fast H atoms with mean kinetic energies ~11 000 cm^{-1}. For Y = I and Br, this process occurs in competition with prompt C–I and C–Br bond cleavage on another $(n/\pi)\sigma^*$ PES, but no Cl/Cl* products unambiguously attributable to one photon induced C–Cl bond fission are observed from 4-ClPhOH. Differences in fragmentation behaviour at longer excitation wavelengths are more marked. Prompt C–I bond fission is observed following excitation of 4-IPhOH at all $\lambda \leq 330$ nm; the wavelength dependent trends in I/I* product branching ratio, kinetic energy release, and recoil anisotropy suggest that (with regard to C–I bond fission) 4-IPhOH behaves like a mildly perturbed iodobenzene. Br atoms are observed when exciting 4-BrPhOH at long wavelengths also, but their velocity distributions suggest that dissociation occurs after internal conversion to the ground state. O–H bond fission, by tunnelling (as in phenol), is observed only in the cases of 4-FPhOH and, more weakly, 4-ClPhOH. These observed differences in behaviour can be understood given due recognition of (i) the differences in the vertical excitation energies of the C–Y centred $(n/\pi)\sigma^*$ potentials across the series Y = I < Br < Cl and the concomitant reduction in C–Y bond strength, cf. that of the rival O–H bond, and (ii) the much increased spin-orbit coupling in, particularly, 4-IPhOH. The present results provide (another) reminder of the risks inherent in extrapolating photochemical behaviour measured for one molecule at one wavelength to other (related) molecules and to other excitation energies. © *2013 AIP Publishing LLC*. [http://dx.doi.org/10.1063/1.4802058]

I. INTRODUCTION

There is an ever growing recognition of the role of $\pi\sigma^*$ and $n\sigma^*$ excited states in promoting molecular photodissociations. Such states are formed by $\sigma^* \leftarrow \pi$ or $\sigma^* \leftarrow n$ orbital promotions, where the σ^* orbital is anti-bonding with respect to a specific bond. We have recently surveyed and attempted to systematise the gas phase photochemistry displayed by many X–H (X = N, O, S, etc.) bond containing molecules following excitation at near ultraviolet (UV) wavelengths.[1,2] The σ^* orbital of interest often has substantial Rydberg character in the vertical Franck-Condon (vFC) region, but becomes localised on the relevant X–H bond as this extends towards dissociation. Much of the recent upsurge in interest in such systems was initiated by *ab initio* calculations of pyrrole, phenol, and indole – prototypical heteroatom containing aromatic systems that are the chromophores of many biomolecules.[3] Experiments have also been pivotal to advancing our understanding of these processes. In the case of phenols, for example, high resolution H (Rydberg) atom photofragment translational spectroscopy (HRA-PTS) studies have revealed selective branching into specific vibrational levels of the radical products formed upon O–H bond fission.[4–6] The observation of such specific energy disposal provides a detailed insight into the nature of the non-adiabatic couplings promoted at conical intersections (CIs) between the potential energy surfaces (PESs) that control the evolution from photoexcited molecule to asymptotic products.

$\pi\sigma^*$ and $n\sigma^*$ excited states are not restricted to X–H bond containing systems. Halides are another obvious class, exemplified by the alkyl and aryl halides in which the σ^* orbital of interest is localised on the C–Y (Y = halogen) bond, with little or no Rydberg character in the vFC region noted from *ab initio* studies. Photochemical studies of the methyl halides[7–11] (and the yet simpler hydrogen halides[12–14]) serve to illustrate an additional complexity in these systems – the spin-orbit coupling associated with the halogen atom. This complexity is revealed in several ways. The increasing

[a] Present address: Department of Chemistry, Hildebrand Hall, University of California, Berkeley, California 94720, USA.
[b] Present address: Department of Physics and Astronomy, VU University Amsterdam, De Boelelaan 1081, NL-1081 HV, Amsterdam, The Netherlands.
[c] Author to whom correspondence should be addressed. Electronic mail: mike.ashfold@bristol.ac.uk. Tel.: +44 (0)117 928 8312. Fax: +44 (0)117 925 1295.

 © 2013 AIP Publishing LLC

Downloaded 30 Apr 2013 to 137.222.43.31. This article is copyrighted as indicated in the abstract. Reuse of AIP content is subject to the terms at: http://jcp.aip.org/about/rights_and_permissions

strength of spin-orbit coupling across the series F < Cl < Br < I leads to a progressive breakdown in the $\Delta S = 0$ spin selection rule accompanying the $\sigma^* \leftarrow n$ orbital promotion. This breakdown manifests itself through an evident evolution of the wavelength resolved photofragmentation behaviour across a given family of halides, in the relative branching into the two spin-orbit states of the halogen product (the $^2P_{3/2}$ ground state and $^2P_{1/2}$ excited state, henceforth referenced as Y and Y*) and in the recoil velocities and anisotropies of the Y/Y* photoproducts.

The halobenzenes (or aryl halides (PhY)) serve as an exemplar of this evolution. All absorb in the near UV, but the consequences of electronic excitation are very different. The long wavelength electronic absorption spectrum of chlorobenzene (henceforth PhCl) is structured,[15–19] and assigned to the S_1–S_0 transition, with the origin identified at $\lambda = 269.92$ nm. This excitation is predominantly $\pi^* \leftarrow \pi$ in character, with resolvable vibronic structure extending to at least $\lambda \sim 247$ nm.[16] PTS studies at $\lambda = 266$ nm reveal formation of Cl atoms, with a total kinetic energy release (TKER) distribution that peaks close to zero.[20] Such "statistical" energy disposal is characteristic of the fragmentation of highly vibrationally excited ground state molecules, formed following internal conversion (IC) from the photo-prepared S_1 state – a view supported by time resolved pump-probe experiments at 266 nm and at 271 nm,[21–23] and by *ab initio* theory.[24,25] PTS studies of PhCl photolysis at shorter excitation wavelengths ($\lambda = 248$ nm[26] and 193 nm[26,27]) indicate broadly similar behaviour, with the bulk of the available energy (E_{avl}, i.e., the difference between the photon energy, E_{phot}, and the C–Cl bond dissociation energy, D_0(Ph−Cl)), partitioned into internal excitation of the Ph radical product. Ichimura *et al.*[26] report an additional fast component in the Cl recoil velocity distributions at both excitation wavelengths, which they attribute to dissociation on a repulsive excited state PES.

Recent velocity mapped ion-imaging (VMI) studies of the photolysis of iodobenzene (PhI)[28,29] and a range of fluorinated iodobenzenes,[30] in contrast, reveal prompt C–I bond fission following excitation at all wavelengths in the range $325 \geq \lambda \geq 215$ nm. The observation of prompt dissociation at such long wavelengths highlights two key differences between PhI and PhCl. First, the comparative weakness of the C–I bond (cf. the C–Cl bond) leads to a concomitant lowering in energy of the dissociative $n\sigma^*$ (and $\pi\sigma^*$) PESs relative to the bound $\pi\pi^*$ states. Second, the increased spin-orbit coupling in PhI allows direct optical access to the lowest (triplet in the spin-orbit free picture) $n\sigma^*$ states, i.e., to states that are forbidden in PhCl.

The UV photochemistry of bromobenzene (PhBr) has been studied less extensively, but the available data hint at excited state dynamics intermediate between that of PhCl and PhI. Like PhCl, PhBr shows structured electronic absorption and 1+1 resonance enhanced multiphoton ionisation (REMPI) spectra at long wavelengths, with the S_1–S_0 ($^1B_2 - ^1A_1$) origin identified at $\lambda = 270.336$ nm.[31] An early (non-spin-orbit state resolved) PTS study at $\lambda = 266$ nm returned a broad Br product velocity distribution, peaking at TKER ~4000 cm^{-1} (47% of E_{avl} at this wavelength) with an associated recoil anisotropy parameter, $\beta = -0.7 \pm 0.2$.[32] Such energy disposal is consistent with (pre-)dissociation via a repulsive excited state PES – an interpretation supported by the dissociation time constant ($\tau = 28$ ps) determined by time-resolved pump-probe measurements at the same wavelength[21] and by *ab initio* theory.[25] A subsequent VMI study[28] of the Br and Br* products from PhBr photolysis at this same wavelength yielded seemingly contradictory results, however. Analysis of the Br image suggested a bimodal TKER distribution with an associated $\beta = -0.02 \pm 0.01$, dominated by a slow, statistical component, while the yield of Br* products appeared to be negligible. Ground state Br atoms are also dominant in the 234 nm photolysis of PhBr,[33] but most of these products appear with substantial kinetic energy (with a mean TKER corresponding to ~60% of E_{avl}) and positive recoil anisotropy.

The halophenols (YPhOH) present an additional richness, given the presence of C–Y and O–H bonds, both of which could act as centres for $\sigma^* \leftarrow n/\pi$ excitations. We have previously reported high resolution time-of-flight (TOF) measurements of the H atom fragments resulting from UV photolysis of 4- (or *para*-)YPhOH (Y = F and Cl) at many wavelengths in the range $287 > \lambda \geq 216$ nm.[34] H atom loss from 4-FPhOH showed many parallels with that observed previously for bare phenol.[4] TKER spectra measured at $\lambda \geq 238$ nm all show an isotropic feature centred at TKER ~5500 cm^{-1}, with structure attributable to 4-FPhO radical formation in a limited sub-set of vibrational levels. This feature is attributable to initial $\pi^* \leftarrow \pi$ excitation at energies below the $S_1(1^1\pi\pi^*)/^1\pi\sigma^*$ CI, and subsequent O–H bond fission by tunnelling through the barrier under the lower diabats of this CI[3,35,36] to yield H atoms and 4-FPhO radicals in their ground electronic state. Spectra recorded at $\lambda \leq 238$ nm reveal a very different TKER distribution, centred at TKER ~12 000 cm^{-1}; excitation at these short wavelengths is deduced to populate the $^1\pi\sigma^*$ state directly.[36] The photolysis of 4-ClPhOH showed clear similarities when the $^1\pi\sigma^*$ state was directly excited, but (relative to 4-FPhOH) the yield of fast H+4-ClPhO products when exciting at energies below the $S_1(1^1\pi\pi^*)/^1\pi\sigma^*$ CI was much reduced. No H atoms attributable to eventual dissociation on the $^1\pi\sigma^*$ PES were observed when exciting 4-BrPhOH at energies below its $S_1(1^1\pi\pi^*)/^1\pi\sigma^*$ CI. Companion low-level time dependent density functional theory (TD-DFT) calculations suggested competition from the alternative C–Br bond fission channel as a likely explanation for the negligible H atom yield, and that an analogous C–Cl bond fission might explain the weakness of the one photon induced H atom signals observed in the photolysis of 4-ClPhOH at longer wavelengths.[34]

Here, we report use of multiple experimental techniques to test such hypotheses further. UV photo-induced formation of Y and Y* products from jet-cooled samples of 4-IPhOH, 4-BrPhOH, and 4-ClPhOH has been investigated by VMI at many near UV excitation wavelengths. The H atom loss channel from these molecules has been explored further by HRA-PTS methods, and the UV absorption spectra of room temperature gas phase samples of all three molecules are also reported. Our interpretation of the various data is aided by new spin-orbit resolved PE calculations as functions of the

Downloaded 30 Apr 2013 to 137.222.43.31. This article is copyrighted as indicated in the abstract. Reuse of AIP content is subject to the terms at: http://jcp.aip.org/about/rights_and_permissions

C–Y bond stretch coordinate (R_{C-Y}) and spin-orbit free PE calculations in the O–H bond stretch coordinate (R_{O-H}). We conclude by comparing and contrasting the complementary experimental and theoretical data for all three molecules and attempt to rationalise the observed parallels and differences.

II. EXPERIMENTAL

4-IPhOH, 4-BrPhOH, and 4-ClPhOH were obtained from Sigma-Aldrich (≥99% purity) and used as supplied. Vapour phase UV absorption spectra of each were recorded using a static gas cell in a commercial spectrometer. The design and operation of the VMI[37] and HRA-PTS[38] experiments have been described previously, so both are only briefly summarised here, focussing particularly on any novel features. In both experiments, the solid sample of interest was placed in an in-line filter positioned just behind the pulsed valve (it was necessary to heat the 4-IPhOH sample to ∼100 °C for the HRA-PTS experiments) and the prevailing vapour pressure diluted in ∼800 mbar of Ar.

Two frequency doubled Nd-YAG pumped dye lasers were used to generate, respectively, the UV photolysis radiation and the necessary REMPI probe wavelengths for the VMI studies. Y and Y* products were detected using established 2+1 REMPI excitation wavelengths, i.e.: I (303.68 nm), I* (304.02 nm),[39] Br (260.622 nm), Br* (262.548 nm),[40] Cl (235.336 nm), Cl* (235.205 nm).[41] These REMPI probe wavelengths all cause some unwanted photolysis of the respective parent molecules, which was particularly problematic in the case of 4-BrPhOH. The unwanted "one-colour" (i.e., probe laser induced) contribution was removed by operating the photolysis laser at 5 Hz (i.e., at half the repetition rate of the probe laser) and at higher UV pulse energies (e.g., ∼2 mJ pulse^{-1} cf. ∼0.5 mJ pulse^{-1} for the probe laser in the case of the Br and Br* imaging studies from 4-BrPhOH), accumulating the alternate 1- and 2-colour images in separate buffers, and then subtracting one from the other to obtain the required 2-colour "difference" image prior to inversion. The photolysis and probe laser pulses were both linearly polarised, with the respective polarisation vectors, $\boldsymbol{\varepsilon}$, aligned parallel to the front face of the detector.

Y^+ ions resulting from each dissociation/ionization event were imaged, and the resulting images inverted to recover the original 3D velocity distribution as described previously.[29,37] The radius to velocity scaling factors were calibrated by imaging the relevant I, Br, and Cl products from photolysis of IBr and BrCl.[37,42] Product yield versus TKER (P(TKER)) distributions derived from Y^+ image analysis are presented following conversion from velocity into TKER space using Eq. (1) with the assumption that the partner fragment has the mass of the 4-hydroxyphenyl radical (which we write as 4-HOPh in order to distinguish it from the phenol molecule, PhOH, with m_R = 93.11 u) and application of the appropriate ($1/v$) Jacobian

$$\mathrm{TKER} = \frac{1}{2} m_Y \left(1 + \frac{m_Y}{m_R}\right) (v_Y)^2, \qquad (1)$$

where m_Y is the mass of the monitored halogen atom (m_I = 126.90 u, m_{Br} = 78.92 u, m_{Cl} = 34.97 u) and v_Y is the experimentally determined Y/Y* atom velocity. Angular distributions, $I(\theta)$, are obtained by integrating the reconstructed 3D spatial distribution over the chosen spread of speeds at each angle. The resulting distribution is characterised by an anisotropy parameter, β, which takes limiting values of +2 and −1 in the cases that the fragment recoil is parallel ($\theta = 0°$) and perpendicular ($\theta = 90°$) to $\boldsymbol{\varepsilon}$.

For the HRA-PTS studies, TOF spectra of H atoms arising from photolysis of 4-ClPhOH, 4-BrPhOH, and 4-IPhOH were recorded at a range of UV wavelengths.[38] At a few selected wavelengths, spectra were measured with the $\boldsymbol{\varepsilon}$ vector of the photolysis radiation aligned at, respectively, θ = 0°, 54.7°, and 90° to the TOF axis, enabling estimation of β. Measured TOF spectra were again transformed to P(TKER) spectra using Eq. (1) where, in this case, m_Y is the mass of the H atom (1.0079 u), m_R is the mass of the co-fragment (assumed to be the YPhO radical, i.e., 219.00 u (4-IPhO), 172.01 u (4-BrPhO), and 127.54 u (4-ClPhO)), and v_Y is the H atom velocity derived from its measured TOF to a detector located at a known distance from the interaction region.

III. COMPUTATIONAL METHODS

The ground state geometry of each 4-YPhOH molecule was optimized with Møller-Plesset second order perturbation theory (MP2) using a cc-pVTZ basis set on all atoms except for oxygen, where the aug-cc-pVTZ basis set was used.[43] A 46 electron effective core potential was used in the case of I.[44]

Potential energy cuts (PECs) along R_{C-Y} were calculated for the ground (S_0, $^1A'$) and numerous singlet and triplet A' and A'' excited states. All of the nuclear coordinates, apart from the bond extension of interest, were held at that of the ground state MP2 equilibrium geometry, using state-averaged (SA) complete active space self-consistent field (CASSCF). Complete active space with second order perturbation theory (CASPT2) spin-orbit free (SOF) energies were then calculated for all states at these same geometries using the SA-CASSCF as a reference wavefunction. For the CASPT2 calculations, an imaginary level shift of 0.7 a.u. was required to avoid intruder state problems. The SA-CASSCF and CASPT2 calculations both employed the same cc-pVTZ basis set used in the MP2 calculations and a 12 electrons in 10 orbitals (12/10) active space. The active space comprised the two lone pairs on the Y atom, three Ph π orbitals, σ and σ^* orbitals associated with the C–Y bond and three π^* orbitals. Spin-orbit coupled (SOC) states were calculated by evaluating $\hat{H}_{SO}$ in a basis of ψ_{elec}; these are henceforth labelled using the extended irreducible representation including both SOF and spin parts. To allow for some treatment of dynamic correlation, CASPT2 (rather than CASSCF) energies of the SOF states were used in the diagonalisation of the SO coupling matrix. The resulting adiabatic PECs were approximately "re-diabatised" in terms of $\pi\pi^*$, $\pi\sigma^*$, and $n\sigma^*$ states, by inspection of the energies, symmetries, and wavefunction coefficients. The SOC-CASPT2 calculations also return the transition dipole moment (TDM) vector between the excited state of interest and the ground state.

Downloaded 30 Apr 2013 to 137.222.43.31. This article is copyrighted as indicated in the abstract. Reuse of AIP content is subject to the terms at: http://jcp.aip.org/about/rights_and_permissions

PECs along R_{O-H} for each 4-YPhOH molecule were calculated using a different 12/10 active space; the C–O and O–H σ orbitals, three Ph π and the oxygen centred p_x lone pair orbitals, and three Ph π^* and the σ^* orbital localised across the O–H bond. Again CASPT2(12/10)/cc-pVTZ PECs were calculated based on a SA-CASSCF wavefunction, with the ring structure fixed at the MP2 ground state minimum energy geometry. SOC-CASPT2 potentials were not constructed for the O–H stretch dimension as the effects of spin-orbit coupling in this coordinate were anticipated to be minimal.

All MP2, CASSCF, and CASPT2 *ab initio* calculations were performed in the MOLPRO computational package.[45] DFT using GAUSSIAN,[46] with the B3LYP functional and the 6-311+G** basis set was used to calculate the normal modes of the 4-HOPh and the various 4-YPhO radicals; the (anharmonic) wavenumbers so derived constitute Tables S1 and S2 in the supplementary material.[47]

IV. EXPERIMENTAL AND THEORETICAL RESULTS AND DISCUSSION

A. UV absorption spectroscopy

UV absorption spectra of 4-IPhOH, 4-BrPhOH, and 4-ClPhOH are shown in Fig. 1. The latter two are qualitatively similar to the corresponding spectrum for phenol, but slightly redshifted. Both display vibronic structure at longer wavelengths, and a more intense feature centred at ~220 nm. The absorption spectrum of 4-IPhOH, in contrast, is more reminiscent of that of PhI – exhibiting an intense maximum at λ ~225 nm and a weaker pedestal that stretches to much longer wavelengths. 1+1 REMPI spectra of jet-cooled 4-BrPhOH and 4-ClPhOH at wavelengths near the respective S_1–S_0 origins have been reported previously, yielding term values: T_{00} = 34 794 cm^{-1} (λ = 287.409 nm) for 4-BrPhOH and T_{00} = 34 811 cm^{-1} (λ = 287.265 nm) for 4-ClPhOH.[34] Attempts to record a similar REMPI spectrum for 4-IPhOH were unsuccessful.

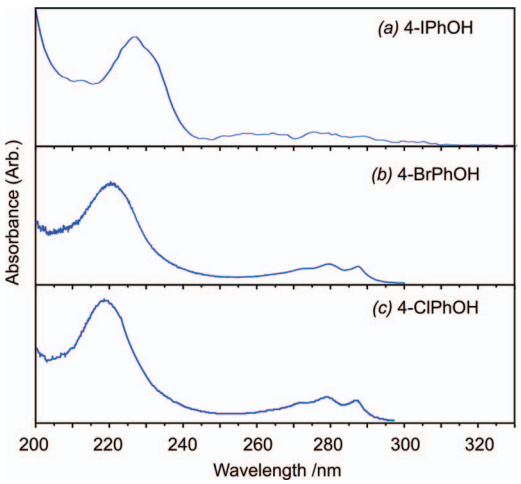

FIG. 1. Room temperature UV absorption spectra of (a) 4-IPhOH, (b) 4-BrPhOH, and (c) 4-ClPhOH vapour recorded in the wavelength range 200 $\leq \lambda \leq$ 330 nm.

B. Y and Y* product forming channels

1. 4-IPhOH

As in our recent VMI studies of the UV photolysis of PhI[29] and various fluorinated iodobenzenes,[30] it proves convenient to start by considering the I* products. Figure 2 shows illustrative data from 4-IPhOH photolysis at (a) 280 nm, (b) 250 nm, (c) 230 nm, and (d) 215 nm. As before,[30] we choose to display the raw image and a 2D slice from the reconstructed 3D distribution in the left and right halves of the left hand panel, and the P(TKER) and β(TKER) distributions of the I*+4-HOPh fragments derived from image analysis on the right. As in the cases of PhI and the various fluorinated iodobenzenes, the longest wavelength image (Fig. 2(a)) shows resolved structure attributable to population of a short progression of vibrational levels of the radical co-fragment. The inter-peak separations (~510 cm^{-1}) match well with the calculated (anharmonic) wavenumber of the a' radical mode ν_{20} (Table S1 in the supplementary material[47]) – the analogue of the in-plane a_1 symmetric ring-breathing mode that is excited in the Ph and 4-FPh products from long wavelength photolysis of PhI and 4-FPhI. This assignment is shown by the comb festooned above the P(TKER) distribution in Fig. 2(a). Associating the peak at highest TKER (TKER$_{max}$) with I* products

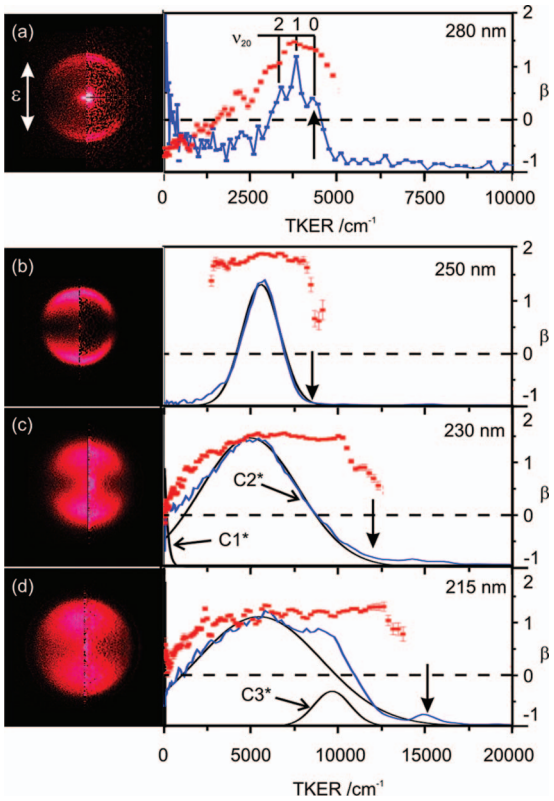

FIG. 2. Raw (left half) and reconstructed slice (right half) images of I* products resulting from photolysis of 4-IPhOH at (a) 280, (b) 250, (c) 230, and (d) 215 nm. $\boldsymbol{\varepsilon}$ is vertical, in the plane of the page. The respective P(TKER) distribution derived from each image is shown alongside (in blue), along with its decomposition into Gaussian components C1*–C3* (shown in black), as are the β(TKER) values derived from analysis of each pixel radius within the reconstructed image (red points, right hand vertical scale). The vertical arrow in each panel indicates TKER$_{max}$, assuming one photon dissociation and D_0(4-HOPh–I) = 23 800 cm^{-1}.

Downloaded 30 Apr 2013 to 137.222.43.31. This article is copyrighted as indicated in the abstract. Reuse of AIP content is subject to the terms at: http://jcp.aip.org/about/rights_and_permissions

formed in association with 4-HOPh radicals in their ground vibrational state allows estimation of the C–I bond strength, $D_0(\text{4-HOPh}-\text{I}) = 23\,800 \pm 150\ \text{cm}^{-1}$ via the relation

$$D_0(\text{4-HOPh}-\text{I}) = E_{\text{phot}} - \text{TKER}_{\text{max}} - A(\text{I}), \qquad (2)$$

where E_{phot} is the photolysis photon energy, A(I) is the spin-orbit splitting of the iodine atom (7603 cm^{-1}, Ref. 48), and the quoted uncertainty on the bond strength corresponds to one pixel at the image radius of interest. The vertical arrows on the P(TKER) plots in Fig. 2 indicate the maximum TKER permissible when forming I* products at each E_{phot}.

This structure coalesces into a single broad feature upon tuning to shorter wavelengths (see, e.g., Fig. 2(b)). As before, we decompose the various P(TKER) distributions (by least squares minimisation) into one or more Gaussian functions; all of the deduced trends with change in E_{phot} are broadly parallel to those found for PhI or 4-FPhI. The distributions determined at long wavelength (e.g., Figs. 2(a) and 2(b)) are dominated by a single feature which, again following past precedent, we label the C2* channel.[29,30] The mean TKER of this feature initially increases with increasing E_{phot} but, by $\lambda \sim 230$ nm (Fig. 2(c)), the mean of the P(TKER) distribution stops increasing and the full width half maximum (FWHM) of the distribution becomes noticeably broader. An additional component (labelled C3*) is clearly evident on the high energy side of the P(TKER) distributions measured at yet shorter wavelengths (see, e.g., Fig. 2(d)). Again as in PhI, the I* products display near limiting parallel recoil anisotropy (i.e., $\beta \sim +2$) except at the shortest wavelengths where the value of β has declined to $\sim +1$.

I atom products were imaged at many wavelengths in the range $330 \geq \lambda \geq 220$ nm. Figure 3 shows data for I atoms from 4-IPhOH photolysis at (a) 303.68 nm (i.e., when using the REMPI probe laser only), (b) 290 nm, (c) 270 nm, (d) 250 nm, and (e) 220 nm. Again, we choose to show the raw image, a 2D slice from the reconstructed 3D distribution and the P(TKER) and β(TKER) distributions derived from image analysis. The parallels between these data and that reported previously for PhI, 4-FPhI, etc., are striking. The P(TKER) distribution measured at 303.68 nm is very similar to that for the I + Ph products from PhI photolysis at this same wavelength[29] and, as before, can be decomposed into contributions from three overlapping Gaussians which we label C3, C2, and C1 (in order of decreasing mean energy) as shown in Fig. 3(a). As in PhI, the C3 products formed at this wavelength display preferential parallel recoil anisotropy ($\beta \sim +1$), and most of E_{avl} (i.e., $E_{\text{phot}} - D_0(\text{4-HOPh}-\text{I})$), is partitioned into product translation. The relative importance of the C1 and C2 product channels declines on tuning to shorter photolysis wavelengths, and the recoil anisotropy of the C3 products changes sign (approaching $\beta = -1$) by $\lambda = 290$ nm (Fig. 3(b)) – behaviour reminiscent of that observed for the C3 products from 4-FPhI photolysis at slightly shorter wavelengths ($\lambda \sim 280$ nm).[30] C3 products continue to dominate at $\lambda = 270$ nm (Fig. 3(c)), but their recoil velocity distribution is now rather isotropic.

Trends apparent upon tuning to yet shorter wavelengths include: (i) the appearance of a new, faster feature (C4) in images recorded in the range $265 \geq \lambda \geq 235$ nm (see, e.g., Fig. 3(d)); (ii) a recovery in the relative importance of the slow (C1/C2) product channels; (iii) the mean TKER of the C3 products, ⟨TKER(C3)⟩, settles on a constant value of $\sim 8000\ \text{cm}^{-1}$ and broadens; and (iv) β(C3) increases, reaching a value of $\sim +1$ by $\lambda = 240$ nm. All of these trends parallel behaviour observed in the UV photolysis of PhI, 4-FPhI, etc., as illustrated in Fig. 4. Figures 4(a) and 4(c) highlight the similar way in which ⟨TKER(C3)⟩ in the UV photolysis of 4-IPhOH and 4-FPhI varies with E_{avl}. As in PhI,[29] the bulk of E_{avl} following long wavelength photolysis is partitioned into product translation but, upon tuning to shorter wavelengths, much of the additional energy provided by the photon is retained as internal excitation of the radical fragment. Figures 4(b) and 4(d) highlight the similarities in the way ⟨β(C3)⟩ (the mean of the β(TKER) values obtained by analysis of each pixel radius over the FWHM of any given C3 feature) varies with E_{avl} for these same two molecules. Both start strongly positive at long wavelengths, dip to negative values at $E_{\text{avl}} \sim 11\,000\ \text{cm}^{-1}$ but then gradually recover to $\langle\beta\rangle > +1$ at the shortest wavelengths investigated.

The evident similarities between 4-IPhOH and 4-FPhI are not restricted to the experimental data. The calculated PECs along $R_{\text{C–I}}$ for these two systems are also very similar, as can be seen by comparing the properties of the SOC states and

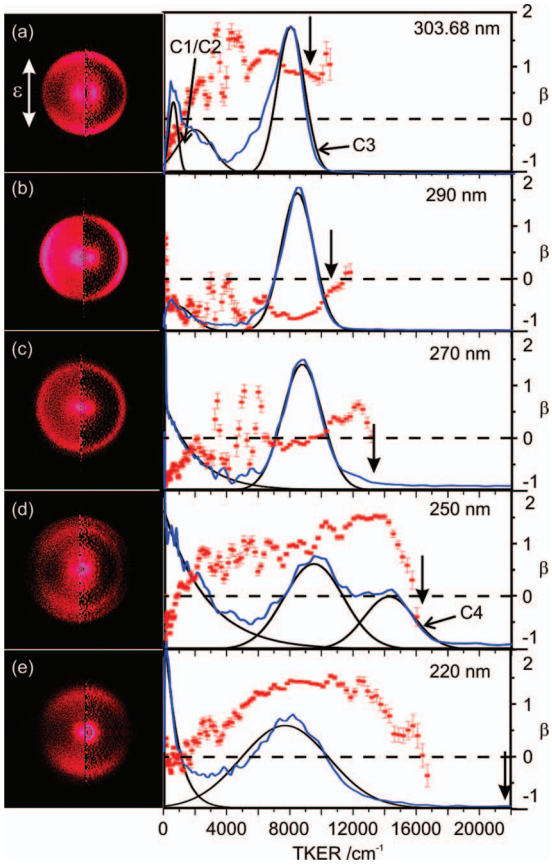

FIG. 3. Raw (left half) and reconstructed slice (right half) images of I products resulting from photolysis of 4-IPhOH at (a) 303.68, (b) 290, (c) 270, (d) 250, and (e) 220 nm. The respective P(TKER) distribution derived from each image is shown alongside (in blue), along with its decomposition into Gaussian components C1–C4 (shown in black). All other details are as for Fig. 2.

Downloaded 30 Apr 2013 to 137.222.43.31. This article is copyrighted as indicated in the abstract. Reuse of AIP content is subject to the terms at: http://jcp.aip.org/about/rights_and_permissions

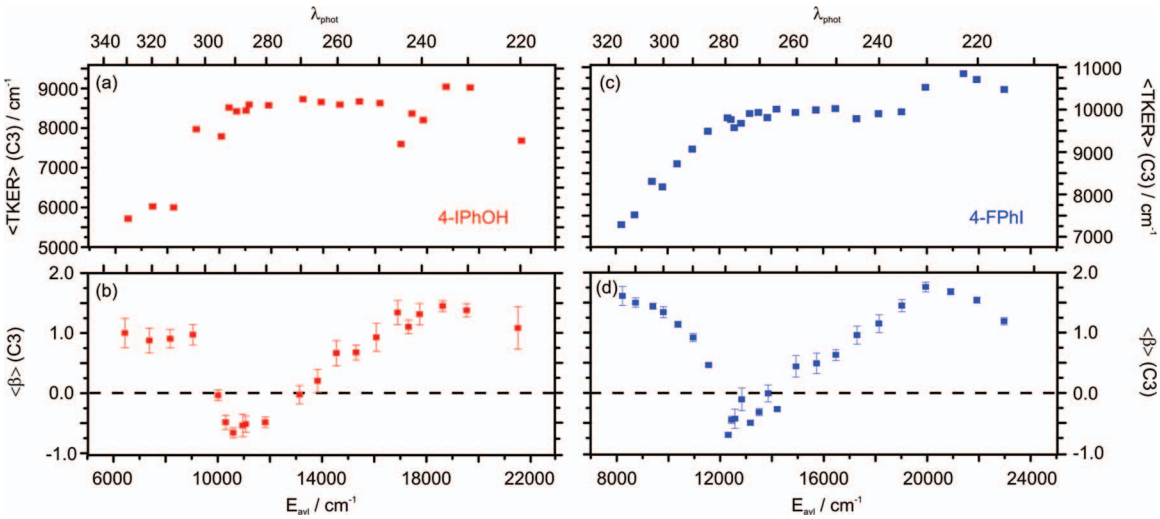

FIG. 4. Plots showing the E_{avl} (and corresponding λ_{phot}, top axes) dependence of the mean TKER of the C3 products in the decomposed P(TKER) distributions from photolysis of (a) 4-IPhOH and (c) 4-FPhI. Panels (b) and (d) compare the E_{avl} dependence of $\langle\beta\rangle$ for the C3 products from these same photolyses. The $\langle\beta\rangle$ values and their corresponding $\pm1\sigma$ errors were obtained by averaging the β(TKER) values derived from analysis of each pixel radius over the FWHM of the C3 feature.

the associated PECs for 4-IPhOH (calculated at the SOC-CASPT2(12/10)/cc-PVTZ level, and presented as Table S3 and Fig. S1 in the supplementary material[47]) with those reported previously for 4-FPhI.[30] Given these parallels, it is appropriate simply to reprise the interpretations of the various product channels observed in the photolysis of 4-FPhI. Channels C1 and C2, which contribute significantly at the longest excitation wavelengths, are explained by initial excitation to the lowest cluster of $\pi\pi^*$ (the $1A''$, $2A''$, and $2A'$) states, which predissociate by coupling with one or more of the repulsive $(n/\pi)\sigma^*$ states (the $3A''$, $3A'$, and $4A'$ states) that correlate with ground state products. The fact that these products appear at such low TKER implies a propensity for E_{avl} mapping through as vibrational excitation of the radical fragment – as observed, and discussed, in the study of PhI photolysis.[29]

The energy disposal in the C3 (and, when active, the C4) product channels is very different from that observed for channels C1/C2. At the longest excitation wavelengths, most of E_{avl} is released as product translation and the C3 products show (non-limiting) parallel recoil anisotropy – both of which characteristics are consistent with excitation to (and dissociation on) the $3A'$ PES, the probability of which is assumed to be boosted by intensity stealing from the "bright" $10A'$ ($\pi\pi^*$) state (as deduced in the case of PhI[29]). The product channel labelled C3 persists to the shortest wavelengths investigated but, as Fig. 4 showed, the recoil anisotropy passes through a local minimum (where $\langle\beta$(C3)$\rangle$ approaches -1), then recovers, and much of the additional energy available as a result of increasing E_{phot} is partitioned into internal excitation of the radical partner. The fall in $\langle\beta$(C3)$\rangle$ coincides in energy with that predicted for the second cluster of $\pi\pi^*$ excited states (the $4A''$, $5A''$, and $5A'$ states). The TDM to each of these states is perpendicular (or near perpendicular) to the C–I bond (see Table S3 in the supplementary material)[47] and, as in 4-FPhI,[30] we explain the localised dip in $\langle\beta$(C3)$\rangle$ by assuming that these $\pi\pi^*$ states provide enhanced transition probability to the same symmetry $(n/\pi)\sigma^*$ continua at these energies. $\langle\beta$(C3)$\rangle$ reverts to positive values as E_{phot} is increased further. I* product formation via channel C2* is also observed at these wavelengths – a signifier of absorption to, and dissociation on, the $8A'$ PES (see below) – and, as in the case of PhI, 4-FPhI, etc., we assume that the C3 product yield at shorter wavelengths is boosted by absorption to the $8A'$ state and subsequent coupling to the $10A''$ and $9A'$ states (analogous to the classic $^3Q_{0+} \rightsquigarrow {}^1Q_1$ radiationless transfer first advanced by Mulliken in the context of the alkyl iodides[49]). C4 products are also assumed to arise as a result of initial population of the $8A'$ state and, in this case, subsequent coupling to $9A''$ PES at shorter R_{C-I} bond lengths.[30]

The I* yield is dominated by C2* products. The observed energy disposal and essentially limiting parallel recoil anisotropy can be understood in terms of population of the $8A'$ PEC and subsequent direct dissociation to 4-HOPh+I* products, with any parent vibrational motions orthogonal to this dissociation coordinate introduced in the initial photoexcitation process carrying through into the radical fragment. Additional fast (C3*) products are observed at the highest E_{phot} and, as with PhI and 4-FPhI, it is likely that these arise following initial population of the strongly absorbing $10A'(\pi\pi^*)$ state and subsequent coupling to one or more of the repulsive $(n/\pi)\sigma^*$ potentials correlating to the 4-HOPh+I* limit.[30]

2. 4-BrPhOH

Images of Br and Br* products were taken following excitation of 4-BrPhOH at many wavelengths in the range $287.6 \geq \lambda \geq 206$ nm. Figure 5 shows selected Br images (raw data and 2D slice, as in Fig. 2) recorded at λ = (a) 287.41 nm, (b) 260.622 nm, (c) 240 nm, (d) 230 nm, and (e) 210 nm, along with the respective P(TKER) and β(TKER) distributions (solid curves and red points, respectively). The 260.622 nm image (Fig. 5(b)) is from a one-colour experiment at the REMPI probe wavelength for ground state Br

Downloaded 30 Apr 2013 to 137.222.43.31. This article is copyrighted as indicated in the abstract. Reuse of AIP content is subject to the terms at: http://jcp.aip.org/about/rights_and_permissions

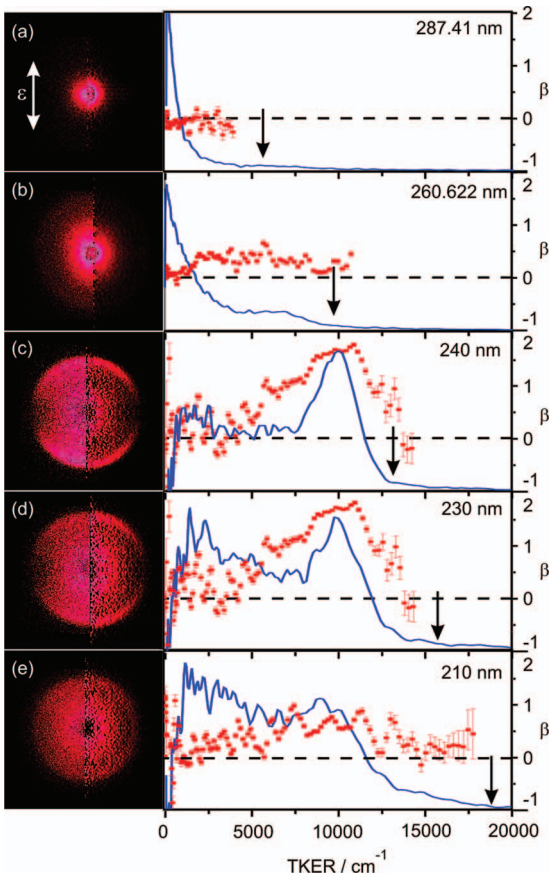

FIG. 5. Raw (left half) and reconstructed slice (right half) images of Br products resulting from photolysis of 4-BrPhOH at (a) 287.41, (b) 260.622, (c) 240, (d) 230, and (e) 210 nm. The respective P(TKER) and β(TKER) distributions derived from each image are shown alongside (solid curves and red points, respectively), along with a vertical arrow indicating $\mathrm{TKER_{max}}$ on the assumption that D_0(4-HOPh−Br) = 28 700 cm^{-1}. All other details are as for Fig. 2.

atoms, whereas the other four are difference images obtained by subtracting images taken with and without the photolysis laser pulse.

The Br atoms formed following excitation on the S_1–S_0 origin (λ = 287.41 nm), or on any of the neighbouring S_1–S_0 resonances to higher energy, show isotropic recoil velocity distributions peaking at zero TKER (see, e.g., Fig. 5(a)). An additional weak feature at higher TKER is evident by λ ~270 nm (see Fig. 5(b)) but this, too, is isotropic. The relative intensity of the feature at higher TKER increases markedly once $\lambda \leq$ 245 nm (Figs. 5(c) and 5(d)), and the associated β value approaches +2 – i.e., the fast Br atoms recoil parallel to $\boldsymbol{\varepsilon}$, implying that the TDM responsible for these products is aligned parallel to the dissociating C–Br bond. Inspection of Fig. 5 suggests that the slow component within the P(TKER) distribution changes also, but we caution that the signal-to-noise ratio at low TKER is noticeably poorer (reflecting the fact that this is the region where the one-colour signal from photolysis/ionization at 260.622 nm (that is subtracted prior to display) makes greatest contribution). The form of the P(TKER) distribution changes again once $\lambda \leq$ 220 nm; the relative intensity of the signal at high TKER declines, and the image appears relatively isotropic.

The λ = 240 nm image (Fig. 5(c)) offers a route to estimating an upper limit for the C–Br bond strength. This Br atom image is reminiscent of that observed for ground state I atoms from UV photolysis of 4-IPhOH at wavelengths in the range 290–270 nm (see, e.g., Figs. 3(b) and 3(c)) and of other aryl iodides.[29,30] In all such cases, the C–I bond strength derived from analysis of the structured I* images was found to match well with that obtained by associating the fast edge of the P(TKER) distribution from I atom images recorded at the longer excitation wavelengths with one photon induced formation of the partner radical in its v = 0 level (i.e., with $\mathrm{TKER_{max}}$). A similar analysis of the Br atom image assuming

$$D_0(\text{4-HOPh}-\text{Br}) = E_{\text{phot}} - \mathrm{TKER_{max}} \qquad (3)$$

and the $\mathrm{TKER_{max}}$ value given by vertical arrow in Fig. 5(c) yields a bond strength D_0(4-HOPh−Br) ~28 700 cm^{-1}, in good accord with the literature value.[50] The vertical arrows in the other panels of Fig. 5 indicate the corresponding $\mathrm{TKER_{max}}$ values based on this estimated bond strength.

Weak Br* signals were observed at all wavelengths investigated ($280 \geq \lambda \geq 205$ nm), but only when using significantly higher photolysis and probe laser intensities than those used for imaging the Br atoms from 4-BrPhOH. The P(TKER) distributions derived from analysis of these images all extend well beyond the expected $\mathrm{TKER_{max}}$ (assuming a one photon dissociation process and A(Br) = 3685.24 cm^{-1}), and none show any obvious discontinuity around this TKER value. Thus, we conclude that most (if not all) of the Br* atoms observed following UV excitation of 4-BrPhOH arise via multiphoton processes, and assume that the quantum yield for one photon dissociation of 4-BrPhOH to Br* products is effectively zero throughout this wavelength range.

Figure 6 shows PECs along $R_{\mathrm{C–Br}}$ for the ground and many excited electronic states returned by the SOC-CASPT2(12/10)/cc-pVTZ calculations for energies ≤ 6.0 eV, which resemble the previously reported SOC curves for PhBr calculated with an inferior double ζ basis set.[51] As in the case of PhI,[29] the various fluorinated iodobenzenes[30] and 4-IPhOH (Fig. S1 in the supplementary material),[47] the adiabatic curves returned by the present calculations undergo multiple true and avoided crossings. The same symmetry crossings generally appear to be localised and, to aid interpretation, we display the diabatic states only and show multiply degenerate surfaces by just one curve. Three product asymptotes are evident in Fig. 6. As in 4-IPhOH, seven (in this case all predominantly $n\sigma^*$) dissociative potentials – three A', four A'' – plus the ground state ($1A'$) PEC correlate with the lowest energy products 4-HOPh($\tilde{\mathrm{X}}$)+Br, and a further four $n\sigma^*$ states (two A', two A'') correlate to the 4-HOPh($\tilde{\mathrm{X}}$)+Br* limit. All of these dissociative PECs intersect with the diabatically bound $\pi\pi^*$ states near (or, at higher energies, in) the vFC region. An additional set of ($\pi\sigma^*$) states are identified correlating to the higher energy 4-HOPh($\tilde{\mathrm{A}}$)+Br asymptote (i.e., to 4-HOPh radicals with a singly occupied π rather than a σ orbital). Since A(Br) is only about half the magnitude of A(I), the energy separation between the second (4-HOPh($\tilde{\mathrm{X}}$)+Y*) and third (4-HOPh($\tilde{\mathrm{A}}$)+Y) dissociation asymptotes is greater in 4-BrPhOH than in 4-IPhOH. This reduces the extent of configuration mixing between same symmetry $n\sigma^*$ and $\pi\sigma^*$

Downloaded 30 Apr 2013 to 137.222.43.31. This article is copyrighted as indicated in the abstract. Reuse of AIP content is subject to the terms at: http://jcp.aip.org/about/rights_and_permissions

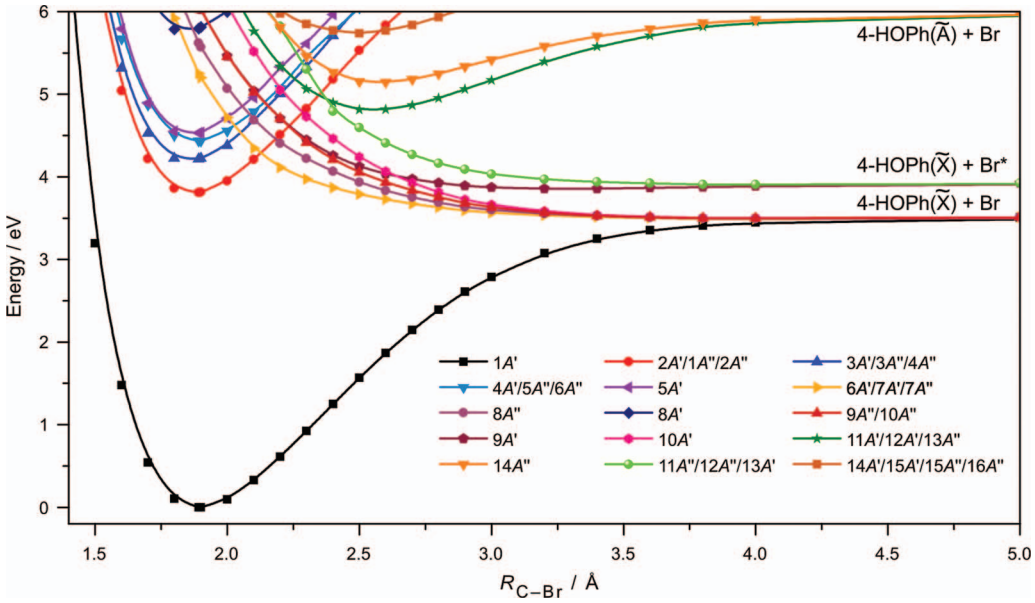

FIG. 6. Spin-orbit resolved PECs for 4-BrPhOH as a function of R_{C-Br}, calculated at the SOC-CASPT2(12/10)/cc-pVTZ level with all other degrees of freedom clamped at the MP2 ground state equilibrium values. The adiabatic outputs have been approximately diabatised by inspecting the energies and wavefunction coefficients.

states converging to these limits and leads to some differences in the energetic ordering of the respective excited states in the vFC region (cf. Tables I and Table S3 in the supplementary material[47]).

Table I lists the vertical excitation energies of the SOC states of 4-BrPhOH (at $R_{C-Br} = 1.892$ Å) and the weightings of the dominant SOF states from which these are derived, along with the calculated TDMs (magnitude and direction, the latter defined with respect to *Z*, the C–Br bond axis). Inspection of Table I shows that, relative to PhI,[29] 4-FPhI,[30] or 4-IPhOH (Table S3 in the supplementary material[47]), there is little singlet-triplet mixing of the SOF wavefunctions in the vFC region; only states that are calculated to be predominantly, if not exclusively, singlet in nature have significant TDMs. Thus, the $5A'$–$1A'$ transition of 4-BrPhOH corresponds to the SOF S_1–S_0 excitation. The SOC-CASPT2/cc-pVTZ calculations return a vertical excitation energy of 4.53 eV for this transition, in good accord with the experimentally determined origin ($T_{00} = 4.31$ eV, Ref. 34).

No fast Br atoms were observed when exciting at the S_1 origin (Fig. 5(a)) – consistent with the PECs in Fig. 6 since the CIs that could enable coupling from the $5A'$ ($\pi\pi^*$) state

TABLE I. SOC state labels, dominant electronic configurations, vertical excitation energies calculated at the equilibrium R_{C-Br} bond length, weights of the respective SOF states from which the SOC states are derived, and transition dipole moments/polarisations calculated for 4-BrPhOH at the SOC-CASPT2(12/10)/cc-pVTZ level of theory. *Z* is aligned with the C–Br bond axis and the ring lies in the *YZ* plane.

State label	Electronic transition	Energy (eV)	Spin-orbit free state	Component TDM (D) (axis)
$2A'$	$\pi\pi^*$	3.81	100% $^3A'$	0.002 (Y)
$1A''$	$\pi\pi^*$	3.81	99.9% $^3A'$	0.000
$2A''$	$\pi\pi^*$	3.81	99.9% $^3A'$	0.002 (X)
$3A'$	$\pi\pi^*$	4.22	100% $^3A'$	0.000
$3A''$	$\pi\pi^*$	4.22	99.3% $^3A'$	0.000
$4A'$	$\pi\pi^*$	4.23	100% $^3A'$	0.000
$4A''$	$\pi\pi^*$	4.42	99.3% $^3A'$	0.000
$5A''$	$\pi\pi^*$	4.43	99.3% $^3A'$	0.429 (X)
$6A''$	$\pi\pi^*$	4.43	99.3% $^3A'$	0.000
$5A'$	$\pi\pi^*$	4.53	100% $^1A'$	0.400 (Y) + 0.013 (Z)
$6A'$	$n\sigma^*$	5.25	98.4% $^3A''$, 1.6% $^3A'$	0.002 (Y) + 0.025 (Z)
$7A'$	$n\sigma^*$	5.25	99.5% $^3A''$	0.048 (Y) + 0.036 (Z)
$7A''$	$n\sigma^*$	5.25	98.5% $^3A''$, 1.5% $^3A'$	0.000
$8A''$	$n\sigma^*$	5.62	95% $^1A''$, 4.3% $^3A'$	0.429 (X)
$8A'$	$\pi\pi^*$	5.79	99.8% $^3A'$	0.215 (Y) + 3.016 (Z)
$9A'$	$n\sigma^*$	6.08	97.8% $^3A'$, 1.6% $^3A''$	0.003 (Y) + 0.019 (Z)
$9A''$	$n\sigma^*$	6.08	97.9% $^3A'$, 1.6% $^3A'$	0.000
$10A''$	$n\sigma^*$	6.09	95.4% $^3A'$, 4.3% $^1A''$	0.075 (X)

Downloaded 30 Apr 2013 to 137.222.43.31. This article is copyrighted as indicated in the abstract. Reuse of AIP content is subject to the terms at: http://jcp.aip.org/about/rights_and_permissions

to the repulsive $6A'$, $7A'$, and/or $7A''$ ($n\sigma^*$) states lie too high in energy. That the P(TKER) distribution of the observed Br atoms peaks at zero likely implies some probability for IC to high vibrational levels of the S_0 ($1A'$) state, some of which (at least) subsequently decay by C–Br bond fission. A small yield of fast (but isotropic) Br atoms is detected upon increasing E_{phot} (see, e.g., Fig. 5(b)), which we attribute to excitation to $5A'$ levels with sufficient energy (in the appropriate modes) to access one or more of these CIs and dissociate on an $n\sigma^*$ PES.

By $\lambda = 240$ nm, a substantial fraction of the Br products appear with high TKER and near-limiting parallel recoil anisotropy (Fig. 5(c)) – characteristics normally associated with direct dissociation following excitation to a repulsive excited state. Figure 6 and Table I identify three $n\sigma^*$ states (the $6A'$, $7A'$, and $7A''$ states) in the relevant energy region. The present calculations suggest that the $7A'$ state carries the largest TDM, but only the $6A'$–$1A'$ excitation has its TDM aligned parallel to the C–Br bond axis – as required to accommodate the recoil anisotropy ($\beta \sim +2$) of these fast Br atoms. As in the aryl iodides,[29,30] we suggest that the $6A'$–$1A'$ transition gains intensity from the strongly allowed $8A' \leftarrow 1A'$ ($\pi^* \leftarrow \pi$) transition (the analogue of the $10A' \leftarrow 1A'$ excitation in 4-IPhOH). The relative yield of fast Br atoms falls on tuning to yet shorter wavelengths (e.g., $\lambda = 210$ nm, Fig. 5(e)), as does their recoil anisotropy. This further change in dynamics likely reflects direct population of the $8A'$ state, the predissociation of which appears to yield Br atoms along with more vibrationally excited radical fragments. Such an interpretation mimics that offered previously to account for changes in the I atom images from PhI photolysis at similar excitation energies.[29]

We can envision two possible reasons for our failure to discern any Br* products unambiguously attributable to one photon photolysis of 4-BrPhOH. First, the $9A'$ ($n\sigma^*$) state – the first excited state that correlates diabatically with Br* products – lies at significantly higher energy than the analogous PEC in 4-IPhOH (labelled $8A'$ in the latter case) and may be outside the vFC window at all wavelengths studied in the present work. As noted in our previous studies of fluorinated iodobenzenes,[30] the stabilisation of this particular A' PEC is sensitively dependent on the extent of $n\sigma^*/\pi\sigma^*$ configuration mixing, which we deduce to be greater in the aryl iodides than in the aryl bromides. Second, we note that a previous study of PhBr photolysis at 235 nm returned a quantum yield for forming Br* products, $\phi_{Br^*} = [Br^*]/\{[Br]+[Br^*]\} \sim 0.09$[33] (cf. ϕ_{I^*} values ~ 0.3 (at $\lambda = 248$ nm) for PhI and various fluorinated iodobenzenes[30]) hinting that, once populated, the efficiency of radiationless transfer from the $9A'$ state via CIs involving one or more of the PECs correlating to ground state Br atoms may be higher than in the iodobenzenes.

3. 4-ClPhOH

Attempts to image Cl (or Cl*) products at any wavelength were hampered by the very much larger ion signals observed at $m/z \geq 36$, attributable to $C_3H_n^+$ ($n = 0$–3) ions. Even the "cleanest" images (the one-colour images taken at the Cl/Cl* REMPI probe wavelengths at 235.336 nm and 235.205 nm) were small and featureless, and required use of significantly higher laser intensities than in the other studies reported here in order to see any Cl/Cl* signals at all. As with the Br* images discussed above, however, the P(TKER) distributions derived from these images stretched well beyond (and showed no obvious step at) the $TKER_{max}$ value expected on the basis of D_0(4-HOPh−Cl) = 33 500 cm^{-1} (Ref. 50), encouraging the view that the observed signals are multiphoton in origin and that the Cl/Cl* atom yield from photolysis of 4-ClPhOH (at this wavelength at least) is small. This is consistent with the calculated SOC-CASPT2/cc-pVTZ PECs in the C–Cl stretch coordinate (Table S4 and Fig. S2 in the supplementary material[47]), which predict that the vertical excitation energy to the first set of dissociative $(n/\pi)\sigma^*$ states is >6 eV.

C. H atom product forming channels

1. HRA-PTS studies of O–H bond fission in 4-YPhOH

Contrary to our earlier investigation,[34] the present studies succeeded in measuring TOF spectra of H atoms from UV photolysis of 4-BrPhOH (and 4-IPhOH). Illustrative P(TKER) spectra for both molecules following excitation at three different wavelengths are shown in Fig. 7. The left hand column shows data from 4-IPhOH, taken at λ = (a) 270 nm, (b) 240 nm, and (c) 220 nm. The first of these panels shows a broad distribution, peaking at TKER $\sim$2000 cm^{-1} and extending to $\sim$14 000 cm^{-1}, the intensity of which is insensitive to the alignment of $\boldsymbol{\varepsilon}$ relative to the TOF axis (i.e., these H atoms display an isotropic recoil velocity distribution). Similar P(TKER) distributions were obtained at all excitation wavelengths $\lambda > 245$ nm, and are regarded as characteristic of H atoms formed by statistical unimolecular decay following IC to high levels of S_0 and/or from unintended multiphoton excitations. Importantly, Fig. 7(a) shows no resolved structure at TKER $\sim$5000 cm^{-1}, such as might be expected (by analogy with PhOH, 4-FPhOH, etc.) if O–H bond fission by tunnelling under one (or more) of the $\pi\pi^*/\pi\sigma^*$ CIs were active fragmentation pathways.[36] An additional fast peak is evident in TKER spectra recorded at $\lambda \leq 245$ nm, however (see, e.g., Figs. 7(b) and 7(c)).

Analogous data for photolysis of 4-BrPhOH at λ = (d) 287.41 nm (resonant with the S_1–S_0 origin), (e) 240 nm, and (f) 220 nm are shown in the right hand panels of Fig. 7. Again, the spectrum taken at longest wavelength shows no structure attributable to excited state O–H bond fission, whereas all spectra taken at $\lambda \leq 245$ nm show a fast feature centred at TKER $\sim$11 000 cm^{-1}. Such features are analogous to those reported from photolysis of 4-FPhOH and 4-ClPhOH at similarly short UV wavelengths[34] and, as in those cases, are attributable to dissociation on a low lying $\pi\sigma^*$ PES in the O–H bond stretch co-ordinate.[36] For both 4-BrPhOH and 4-IPhOH, the envelope at high TKER observed upon short wavelength excitation shows poorly resolved structure (see insets to panels (b) and (e) in Fig. 7), which we tentatively assign to short progressions in 4-YPhO radical modes ν_{9b} (the in-plane C–O/C–Y wagging mode) and ν_{18b} (the in-plane C–O wag). Analogy with PhOH[4] and 4-FPhOH[34] suggests that these

Downloaded 30 Apr 2013 to 137.222.43.31. This article is copyrighted as indicated in the abstract. Reuse of AIP content is subject to the terms at: http://jcp.aip.org/about/rights_and_permissions

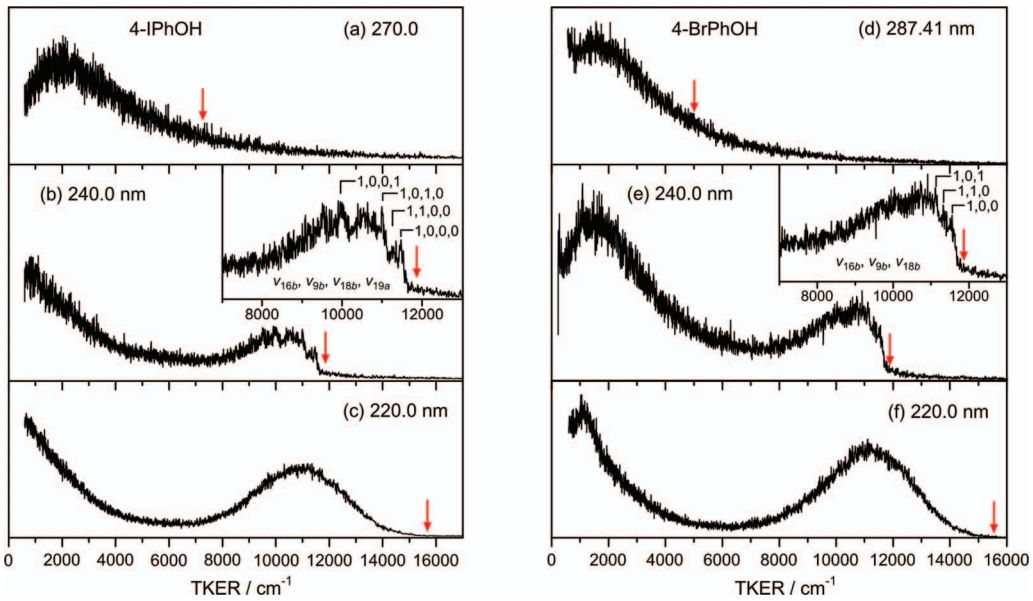

FIG. 7. *P*(TKER) spectra derived from H atom TOF spectra measured following photolysis of 4-IPhOH at λ = (a) 270, (b) 240, and (c) 220 nm and of 4-BrPhOH at λ = (d) 287.41, (e) 240, and (f) 220 nm. The vertical arrows indicate the $TKER_{max}$ value permitted by one photon induced O–H bond fission at each photolysis wavelength assuming D_0(4-IPhO−H) = 29 770 ± 100 cm^{-1} and D_0(4-BrPhO−H) = 29 790 ± 100 cm^{-1}. The insets in panels (b) and (e) show tentative product mode assignments involving single quanta of ν_{9b}, ν_{18b}, and ν_{19a} (panel (b)) and ν_{9b} and ν_{18b} (panel (e)), all built on a quantum of ν_{16b}.

progressions are likely built on one quantum of ν_{16b} (which is deduced to act as a promoting mode in the initial excitation step and carries through into the radical product). That being so, and using the appropriate ν_{16b} wavenumbers listed in Table S2 in the supplementary material,[47] we deduce O–H bond strengths D_0(4-BrPhO−H) = 29 790 ± 100 cm^{-1} and D_0(4-IPhO−H) = 29 770 ± 100 cm^{-1} that match sensibly with D_0(4-FPhO−H) = 29 370 ± 50 cm^{-1} and D_0(4-ClPhO−H) = 29 520 ± 50 cm^{-1} (Ref. 34) (cf. D_0(PhO−H) = 30 015 ± 40 cm^{-1}) and imply that the smaller Y substituents offer some modest stabilisation of the resulting radical.[6] The vertical arrow in each panel of Fig. 7 indicates the $TKER_{max}$ value permitted by one photon induced O–H bond fission at each photolysis wavelength given these bond strengths.

H atom TOF spectra from photolysis of 4-ClPhOH have been reported previously at many wavelengths between λ = 287.241 nm (the S_1–S_0 origin) and 216 nm.[34] TKER spectra obtained at just three wavelengths within the S_1–S_0 absorption feature showed vestigial structure at TKER ~5300 cm^{-1}, attributable to H+4-ClPhO($\tilde{X}$) radical formation by tunnelling under the $S_1/^1\pi\sigma^*$ CI. TKER spectra obtained from H atom TOF measurements at $\lambda_{phot} \leq 238$ nm, in contrast, all show a structured component centred at

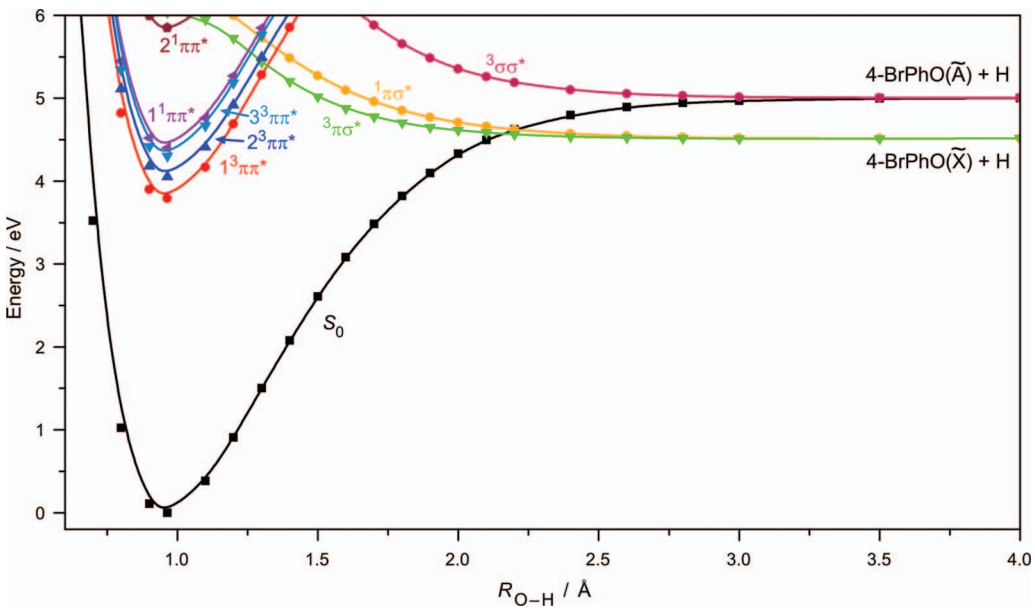

FIG. 8. Spin-orbit free PECs for 4-BrPhOH as a function of R_{O-H}, calculated at the CASPT2(12/10)/cc-pVTZ level, with all other degrees of freedom held at their MP2 ground state equilibrium values.

Downloaded 30 Apr 2013 to 137.222.43.31. This article is copyrighted as indicated in the abstract. Reuse of AIP content is subject to the terms at: http://jcp.aip.org/about/rights_and_permissions

$\sim$11 500 cm^{-1} – analogous to that from 4-BrPhOH and 4-IPhOH at similarly short wavelengths (see, e.g., Figs. 7(b), 7(c), 7(e), and 7(f)) – which we attribute to dissociation on the $^1\pi\sigma^*$ PES.

2. Spin-orbit free PECs along R_{O-H}

Figure 8 shows calculated spin-orbit free PECs for 4-BrPhOH along the R_{O-H} coordinate, calculated at the CASPT2(12/10)/cc-pVTZ level. The singlet PECs are reassuringly similar to those derived from similar calculations for bare phenol.[36] As noted in Ref. 6, rigid scans such as these (i.e., where all degrees of freedom apart from R_{O-H} are held fixed at their ground state equilibrium values) consistently overestimate D_0(4-YPhO–H) and thus the area of the barrier under the $S_1/^1\pi\sigma^*$ CI. Correcting these *ab initio* PECs as in Ref. 6 suggests that the barrier to tunnelling on the singlet PESs will increase in the order 4-ClPhOH < 4-BrPhOH < 4-IPhOH (reflecting the modest increase in bond strength), and that the probabilities of O–H bond fission by tunnelling through this barrier will thus decrease with increasing mass of Y. Our recent tunnelling calculations[6] suggest that the O–H bond fission rate by tunnelling from the S_1 state of 4-ClPhOH is $\sim$100-fold less than that from the S_1 state of bare PhOH (the latter is estimated at $\sim 10^8$–10^9 s^{-1}); the present study implies that the corresponding tunnelling rates in 4-BrPhOH and 4-IPhOH will be slower still, though we recognise that the increase in spin-orbit coupling (particularly in the latter case) might enable some contribution from tunnelling to the $^3\pi\sigma^*$ PES.

V. CONCLUSIONS

The present combined experimental and theoretical study reveals a systematic evolution in photofragmentation behaviour across the family of 4-YPhOH molecules as Y is changed from I through Br to Cl (and F[34]). At short wavelengths (below $\sim$240 nm), all show clear evidence of O–H bond fission on a repulsive ($\pi\sigma^*$) PES, yielding fast H atoms with an associated $\langle$TKER$\rangle$ $\sim$11 000 cm^{-1}. In the cases that Y = I and Br, at least, this process is occurring in competition with fast C–I and C–Br bond fission on another $(n/\pi)\sigma^*$ PES – as revealed by the anisotropic distributions of recoiling I (and I*) and Br atom fragments. However, the *P*(TKER) distributions of these Y/Y* fragments show no obvious wavelength dependence consistent with the energetic onset of the competing O–H bond fragmentation. No Cl/Cl* products unambiguously attributable to one photon induced C–Cl bond fission were observed at any excitation wavelength. This might simply reflect the rather poor signal-to-noise ratios associated with Cl atom detection in the present studies, but is also generally consistent with the previous studies of PhCl photochemistry which suggested IC to S_0 as the dominant excited state decay process.[22,23]

Photochemical differences at long excitation wavelengths are much more marked. One key factor is the change in C–Y bond strength relative to that of the O–H bond; D_0(4-HOPh−I) is $\sim$6000 cm^{-1} lower than D_0(4-IPhO−H), D_0(4-HOPh−Br) is $\sim$1000 cm^{-1} less than D_0(4-BrPhO−H) while the C–Cl bond strength in 4-ClPhOH is $\sim$4000 cm^{-1} larger than D_0(4-ClPhO−H). This, combined with the much stronger spin-orbit coupling, ensures absorption by (and some prompt C–I bond fission from) 4-IPhOH at all wavelengths $\leq$330 nm – thereby explaining the anisotropic I atom recoil velocity distributions and our inability to measure a structured parent REMPI excitation spectrum at these wavelengths. The wavelength dependent trends in *P*(TKER) and β(TKER) for the I and I* product channels are very similar to those reported previously for molecules like 4-FPhI. O–H bond fission at these wavelengths, in contrast, would involve tunnelling through the barrier under the $\pi\pi^*/\pi\sigma^*$ CI in the R_{O-H} coordinate. Comparison with the corresponding PECs for PhOH, etc.,[6] suggests that the rate for this process will be $\ll 10^9$ s^{-1}, which explains our non-observation of one photon induced O–H bond fission products at low E_{phot}. Photochemically, 4-IPhOH behaves like a mildly perturbed iodobenzene at long wavelengths.

The *ab initio* calculations show spin-orbit coupling to be much weaker in 4-BrPhOH, and the longest wavelength absorption is to the $S_1(^1\pi\pi^*)$ state. The S_1–S_0 absorption and parent REMPI excitation spectra of 4-BrPhOH are similar to those of bare phenol. Such findings accord with the observed statistical *P*(TKER) distribution of Br products following excitation at the S_1–S_0 origin, consistent with IC to high vibrational levels of the S_0 state and subsequent unimolecular decay by C–Br bond fission. Fast Br atoms are observed at shorter excitation wavelengths (λ $\sim$240 nm), with β $\sim$+2 and a *P*(TKER) distribution consistent with prompt dissociation on the $6A'$ PES, but the appearance (and weakness) of the Br* images at all wavelengths investigated suggests that the quantum yield for one photon dissociation of 4-BrPhOH to Br* products is effectively zero. Weak H atom signals attributable to tunnelling through the barrier under the $S_1/^1\pi\sigma^*$ CI in the O–H stretch coordinate are observed following excitation to selected levels of the S_1 state of 4-ClPhOH, but this process is deduced to be much less efficient than in 4-FPhOH or PhOH.

The 4-YPhOH molecules display a wide range of photofragmentation behaviour, varying with the choice of Y and/or excitation wavelength. But, as the present study demonstrates, most of the observed variations conform to a self-consistent picture given due recognition of the relative C–Y and O–H bond strengths and the effects of Y substitution on the excited state PESs and TDMs. The present work provides (another) reminder of the potential hazards inherent in extrapolating photochemical behaviour measured for one molecule at one wavelength, to other (related) molecules and to other excitation energies.

ACKNOWLEDGMENTS

The Bristol authors are grateful to the Engineering and Physical Sciences Research Council (U.K.) (EPSRC(GB)) for financial support through a programme grant (EP/G00224X) and to T. Hama (University of Kyoto), R. N. Dixon, S. J. Harris, T. N. V. Karsili, K. N. Rosser, J. A. Smith, and A. M. Wenge for their many and varied contributions to the work

Downloaded 30 Apr 2013 to 137.222.43.31. This article is copyrighted as indicated in the abstract. Reuse of AIP content is subject to the terms at: http://jcp.aip.org/about/rights_and_permissions

described herein. M.N.R.A. is also pleased to acknowledge support through the Marie Curie Initial Training Network (ICONIC, Contract Agreement No. 238671) and is grateful for the award of a Royal Society Leverhulme Trust Senior Research Fellowship.

[1]M. N. R. Ashfold, G. A. King, D. Murdock, M. G. D. Nix, T. A. A. Oliver, and A. G. Sage, Phys. Chem. Chem. Phys. **12**, 1218 (2010).
[2]M. N. R. Ashfold, B. Cronin, R. N. Dixon, A. L. Devine, and M. G. D. Nix, Science **312**, 1637 (2006).
[3]A. L. Sobolewski, W. Domcke, C. Dedonder-Lardeux, and C. Jouvet, Phys. Chem. Chem. Phys. **4**, 1093 (2002).
[4]M. G. D. Nix, A. L. Devine, B. Cronin, R. N. Dixon, and M. N. R. Ashfold, J. Chem. Phys. **125**, 133318 (2006).
[5]M. N. R. Ashfold, A. L. Devine, R. N. Dixon, G. A. King, M. G. D. Nix, and T. A. A. Oliver, Proc. Natl. Acad. Sci. U.S.A. **105**, 12701 (2008).
[6]T. N. V. Karsili, A. M. Wenge, D. Murdock, S. J. Harris, J. N. Harvey, R. N. Dixon, and M. N. R. Ashfold, Chem. Sci. **2013** (published online).
[7]R. O. Loo, H. P. Haerri, G. E. Hall, and P. L. Houston, J. Chem. Phys. **90**, 4222 (1989).
[8]A. T. J. B. Eppink and D. H. Parker, J. Chem. Phys. **110**, 832 (1999).
[9]J. G. Underwood and I. Powis, Phys. Chem. Chem. Phys. **2**, 747 (2000).
[10]M. L. Lipciuc and M. H. M. Janssen, J. Chem. Phys. **127**, 224310 (2007).
[11]Y. Matsumi, P. K. Das, and M. Kawasaki, J. Chem. Phys. **92**, 1696 (1990).
[12]P. M. Regan, S. R. Langford, D. Ascenzi, P. A. Cook, A. J. Orr-Ewing, and M. N. R. Ashfold, Phys. Chem. Chem. Phys. **1**, 3247 (1999).
[13]P. M. Regan, S. R. Langford, A. J. Orr-Ewing, and M. N. R. Ashfold, J. Chem. Phys. **110**, 281 (1999).
[14]P. M. Regan, D. Ascenzi, C. Clementi, M. N. R. Ashfold, and A. J. Orr-Ewing, Chem. Phys. Lett. **315**, 187 (1999).
[15]H. D. Bist, V. N. Sarin, A. Ojha, and Y. S. Jain, Appl. Spectrosc. **24**, 292 (1970).
[16]P. Imhof and K. Kleinermanns, Chem. Phys. **270**, 227 (2001).
[17]Y. S. Jain and H. D. Bist, J. Mol. Spectrosc. **47**, 126 (1973).
[18]T. Cvităs and J. M. Hollas, Mol. Phys. **18**, 101 (1970).
[19]T. G. Wright, S. I. Panov, and T. A. Miller, J. Chem. Phys. **102**, 4793 (1995).
[20]G. J. Wang, R. S. Zhu, H. Zhang, K. L. Han, G. Z. He, and N. Q. Lou, Chem. Phys. Lett. **288**, 429 (1998).
[21]M. Kadi, J. Davidsson, A. N. Tarnovsky, M. Rasmusson, and A. Akesson, Chem. Phys. Lett. **350**, 93 (2001).
[22]B. Liu, B. Wang, Y. Wang, and L. Wang, Chem. Phys. Lett. **477**, 266 (2009).
[23]Y. Z. Liu, C. G. Qin, S. Zhang, Y. M. Wang, and B. Zhang, Acta Physico-Chim. Sin. **27**, 965 (2011).
[24]A. L. Sobolewski and W. Domcke, Chem. Phys. **259**, 181 (2000).
[25]Y.-J. Liu, P. Persson, and S. Lunell, J. Phys. Chem. A **108**, 2339 (2004).
[26]T. Ichimura, Y. Mori, H. Shinohara, and M. Nishi, Chem. Phys. **189**, 117 (1994).
[27]A. Freedman, S. C. Yang, M. Kawasaki, and R. Bersohn, J. Chem. Phys. **72**, 1028 (1980).
[28]X.-P. Zhang, Z.-R. Wei, Y. Tang, T.-J. Chao, B. Zhang, and K.-C. Lin, ChemPhysChem **9**, 1130 (2008).
[29]A. G. Sage, T. A. A. Oliver, D. Murdock, M. D. Crow, G. A. D. Ritchie, J. N. Harvey, and M. N. R. Ashfold, Phys. Chem. Chem. Phys. **13**, 8075 (2011), and references therein.
[30]D. Murdock, M. B. Crow, G. A. D. Ritchie, and M. N. R. Ashfold, J. Chem. Phys. **136**, 124313 (2012).
[31]T. G. Dietz, M. A. Duncan, M. G. Liverman, and R. E. Smalley, J. Chem. Phys. **73**, 4816 (1980).
[32]H. Zhang, R.-S. Zhu, G.-J. Wang, K.-L. Han, G.-Z. He, and N.-Q. Lou, J. Chem. Phys. **110**, 2922 (1999).
[33]D. Paul, H. K. Kim, K. Hong, and T. K. Kim, Bull. Korean Chem. Soc. **32**, 659 (2011).
[34]A. L. Devine, M. G. D. Nix, B. Cronin, and M. N. R. Ashfold, Phys. Chem. Chem. Phys. **9**, 3749 (2007).
[35]G. A. Pino, A. N. Olfdani, E. Marceca, M. Fujii, S.-I. Ishiuchi, M. Miyazaki, M. Broquier, C. Dedonder, and C. Jouvet, J. Chem. Phys. **133**, 124313 (2010).
[36]R. N. Dixon, T. A. A. Oliver, and M. N. R. Ashfold, J. Chem. Phys. **134**, 194303 (2011).
[37]E. Wrede, S. Laubach, S. Schulenburg, A. Brown, E. R. Wouters, A. J. Orr-Ewing, and M. N. R. Ashfold, J. Chem. Phys. **114**, 2629 (2001).
[38]B. Cronin, M. G. D. Nix, R. H. Qadiri, and M. N. R. Ashfold, Phys. Chem. Chem. Phys. **6**, 5031 (2004).
[39]A. Gedanken, M. B. Robin, and Y. Yafet, J. Chem. Phys. **76**, 4798 (1982).
[40]S. Arepalli, N. Presser, D. Robie, and R. J. Gordon, Chem. Phys. Lett. **117**, 64 (1985).
[41]S. Arepalli, N. Presser, D. Robie, and R. J. Gordon, Chem. Phys. Lett. **118**, 88 (1985).
[42]M. J. Cooper, P. J. Jackson, L. J. Rogers, A. J. Orr-Ewing, M. N. R. Ashfold, and B. J. Whitaker, J. Chem. Phys. **109**, 4367 (1998).
[43]T. H. Dunning, Jr., J. Chem. Phys. **90**, 1007 (1989).
[44]M. Dolg, *Habilitationsschrift*, Universität Stuttgart, 1997.
[45]H. J. Werner, P. J. Knowles, G. Knizia, F. R. Manby, M. Schütz *et al.*, MOLPRO, version 2010.1, a package of *ab initio* programs, 2010, see http://www.molpro.net.
[46]M. J. Frisch, G. W. Trucks, H. B. Schlegel *et al.*, GAUSSIAN 03, Revision C.02, Gaussian, Inc., Wallingford, CT, 2004.
[47]See supplementary material at http://dx.doi.org/10.1063/1.4802058 for the calculated anharmonic normal mode wavenumbers of 4-HOPh (Table S1), 4-IPhO, 4-BrPhO, and 4-ClPhO radicals (Table S2), for the analogues of Table I, for the cases of 4-IPhOH (Table S3) and 4-ClPhOH (Table S4), and for plots of the spin-orbit resolved PECs of 4-IPhOH as a function of $R_{C–I}$ (Figure S1) and of 4-ClPhOH as a function of $R_{C–Cl}$ (Figure S2) for energies up to 6 eV.
[48]L. Minnhagen, Ark. Fys. **21**, 415 (1962).
[49]R. S. Mulliken, J. Chem. Phys. **8**, 382 (1940).
[50]E. M. C. Chen, K. Albyn, L. Dussack, and W. E. Wentworth, J. Phys. Chem. **93**, 6827 (1989), and references therein.
[51]S.-F. Chen, F.-Y. Liu, and Y.-J. Liu, J. Chem. Phys. **131**, 124304 (2009).

Downloaded 30 Apr 2013 to 137.222.43.31. This article is copyrighted as indicated in the abstract. Reuse of AIP content is subject to the terms at: http://jcp.aip.org/about/rights_and_permissions